# Searching for dark matter axions via atomic excitations+

J.D. Vergados**,

University of Ioannina

+Work initiated on a visit to:

KAIST University& Center for Axion and Precision Physics Research, IBS, Daejeon, Republic of Korea

**Work done In collaboration with S. Cohen (UoI) and F, Avignone and R. Creswick (USC,USA)

# Why axions? They are expected to exist! (Neutrino History repeated?)

In the standard model there is a source of CP violation from the phase in the Kobayashi-Maskawa mixing matrix.

Another source is the phase θ in the interaction between gluons (θ-parameter), expected to be of order 1.

The non observation of the electric dipole moment of the neutron is a problem.

$$d^n = (3\times10^{-16}\ \text{e-cm})\,\theta \rightarrow$$

Experimentally (Phys. Rev. D 92, 092003 (2015) )

$d^n < 3\times10^{-26}$ e-cm(90% CL) CL)--> $\theta = 10^{-10}$

$d^n < 3.6\times10^{-26}$ e-cm(95% CL)--> $\theta = 1.2\times10^{-10}$

The smallness of θ can be achieved by fine tuning, but this is not acceptable.

The introduction of the axion, a pseudo-scalar field, solves this problem via spontaneous symmetry breaking, i.e.

$$\theta \rightarrow \theta - a/f_a$$

Where a is the axion field and $f_a$ the axion decay constant. Hence the axion field is required.

# Why axions as dark matter candidates?

The relic axions, produced during the QCD phase transition in the early Universe, satisfy all the requirements of dark matter. Thus the hypothetical axion solves simultaneously both the strong CP and dark matter problems.

# Main ways of dark matter axion detection

The axions are extremely light. So it is impossible to detect dark matter axions via scattering them off targets. Thus:

1. They are detected by their conversion to photons in the presence of a magnetic field (Primakoff effect). The produced photons are detected in a resonance cavity. Ongoing searches: (ADMX, CAPP (Korea) etc).

2, The absorption of dark matter axions in atoms (our suggestion). This proceeds via the axion - electron coupling. Stringent experimental limits have appeared for this coupling.

The expected rate is, however, detectable, due to the large axion particle density in the vicinity of the detector as a result of the smallness of the axion mass.

The axion absorption in the presence of a magnetic field leads to resonance behavior.

The characteristics of the resonance depend on the velocity distribution.

Top: Photon to axion conversion (Primakoff effect)

bottom: Axion induced atomic excitation In the presence of B

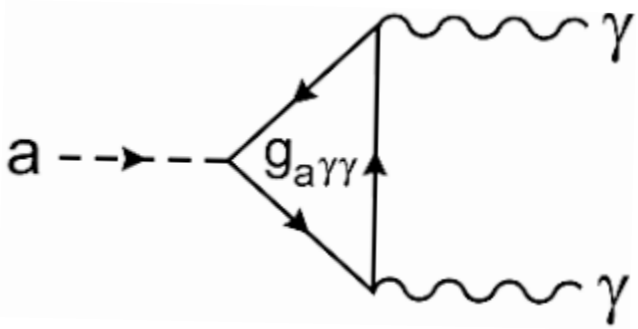


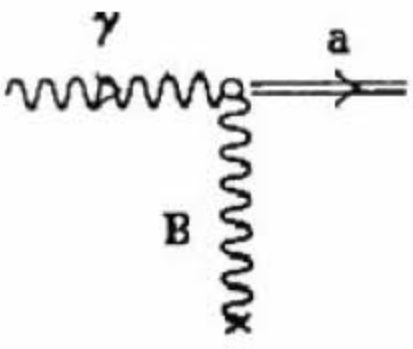


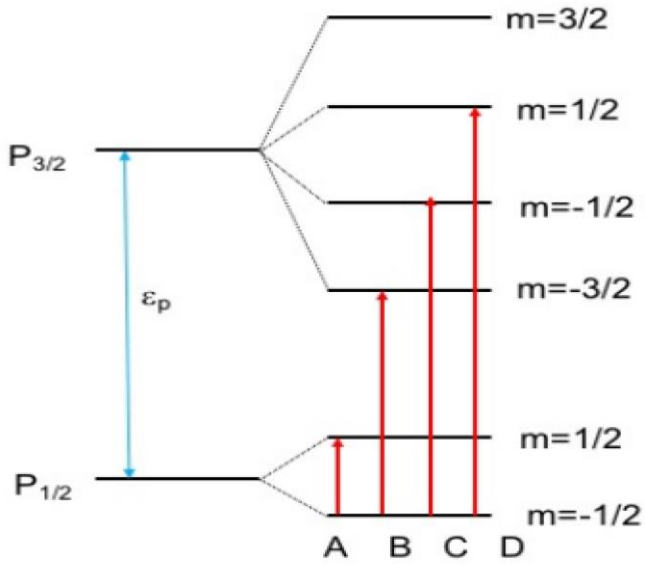


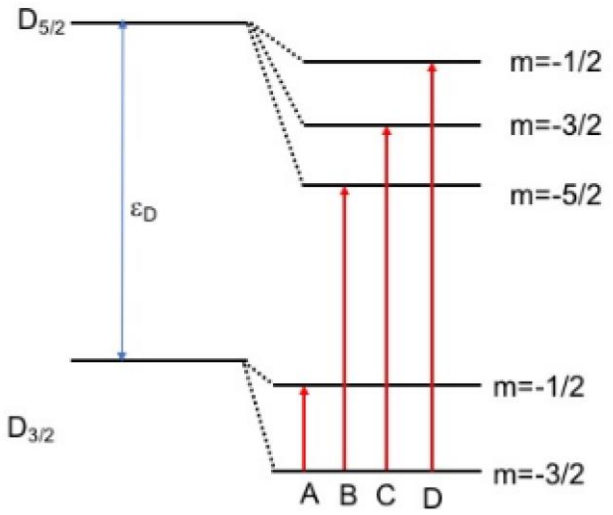

# Axion absorption in atoms: The axion- electron coupling

## (There exists a similar coupling for the quarks)

The axion $a$ is a pseudoscalar particle. We remind the reader that tts coupling to the electron takes the form of an axial current interaction:

$$\mathcal{L} = \frac{g_e}{f_a} i\partial_\mu a \bar{\psi}(\mathbf{p}', s)\gamma^\mu\gamma_5\psi(\mathbf{p}, s)$$

where $g_e$ is a coupling constant and $f_a$ a scale parameter with the dimension of energy. For an axion with mass $m_a$ described by a a plane wave it easy to show:

- the time component $\mu = 0$ is given by:

$$\mathcal{L} = \langle\phi|\Omega|\phi\rangle,\ \Omega = \frac{g_e m_a}{2f_a}\frac{\boldsymbol{\sigma}.\mathbf{q}}{m_e},\ \mathbf{q} = \mathbf{p}' - \mathbf{p}$$

  which is negligible for $m_a << m_e$.

- The space component, $\mu \neq 0$, in the non relativistic limit is given by

$$\mathcal{L}_{aee} = \langle\phi|\Omega|\phi\rangle,\ \Omega = \frac{g_e}{2f_a}\boldsymbol{\sigma}.\mathbf{q}$$

  where $\mathbf{q}$ is the axion momentum.

# - Determination of the axion electron coupling

A crucial parameter in the present work is $\frac{g_{ae}}{f_a}$. In the past this parameter was derived from existing axion models. In a recent paper:
G. Bellini et al. (The Borexino Collaboration), Phys. Rev. D 85, 092003 (2012), arXiv:1203.6258 [hep-ex].
the following limits were obtained:

$$|g_{Ae} \times m_A| \leq 2.0 \times 10^{-5}\text{eV},\ |g_{Ae} \times g_{3AN}| \leq 5.5 \times 10^{-13}\text{eV}. \quad (19)$$

These can be interpreted to be the axion electron and the isovector axion nucleon coupling, which in our notation are written:

$$|g_{ae} \times m_a| \leq 2.0 \times 10^{-5}\text{eV},\ |g^3_{aN}| \leq 2.8 \times 10^{-8}\text{eV} \quad (20)$$

Using now the equation

$$m_a f_a \approx 6000\text{MeV}^2 \quad (21)$$

we obtain

$$\frac{g_{ae}}{f_a} \leq 3.3 \times 10^{-12}\text{GeV}^{-1},\ \frac{g^3_{aN}}{f_a} \leq 4.7 \times 10^{-15}\text{GeV}^{-1} \quad (22)$$

# - The axion – electron coupling (continued)

The axion electron coupling is not known, It has been studied in various axion models, e.g.

M. Dine and W. Fischler, Phys. Lett. B120, 137 (1983).

J. Preskill, M. B. Wise, and F. Wilczek, Phys. Lett. B120, 127 (1983).

They find:

$$g_{ae} = \frac{1}{3}\left(1 - \frac{\tan^2\beta}{1+\tan\tan^2\beta}\right), \tan\beta = \frac{v_2}{v_2} \text{ or } g_{ae} = \frac{1}{3}\cos^2\beta \quad (23)$$

Where $\tan\beta$ is the ratio of the vacuum expectation values of the two doublets of the model, the parameter $\beta$ is not known.

# - The allowed range of the axion masses

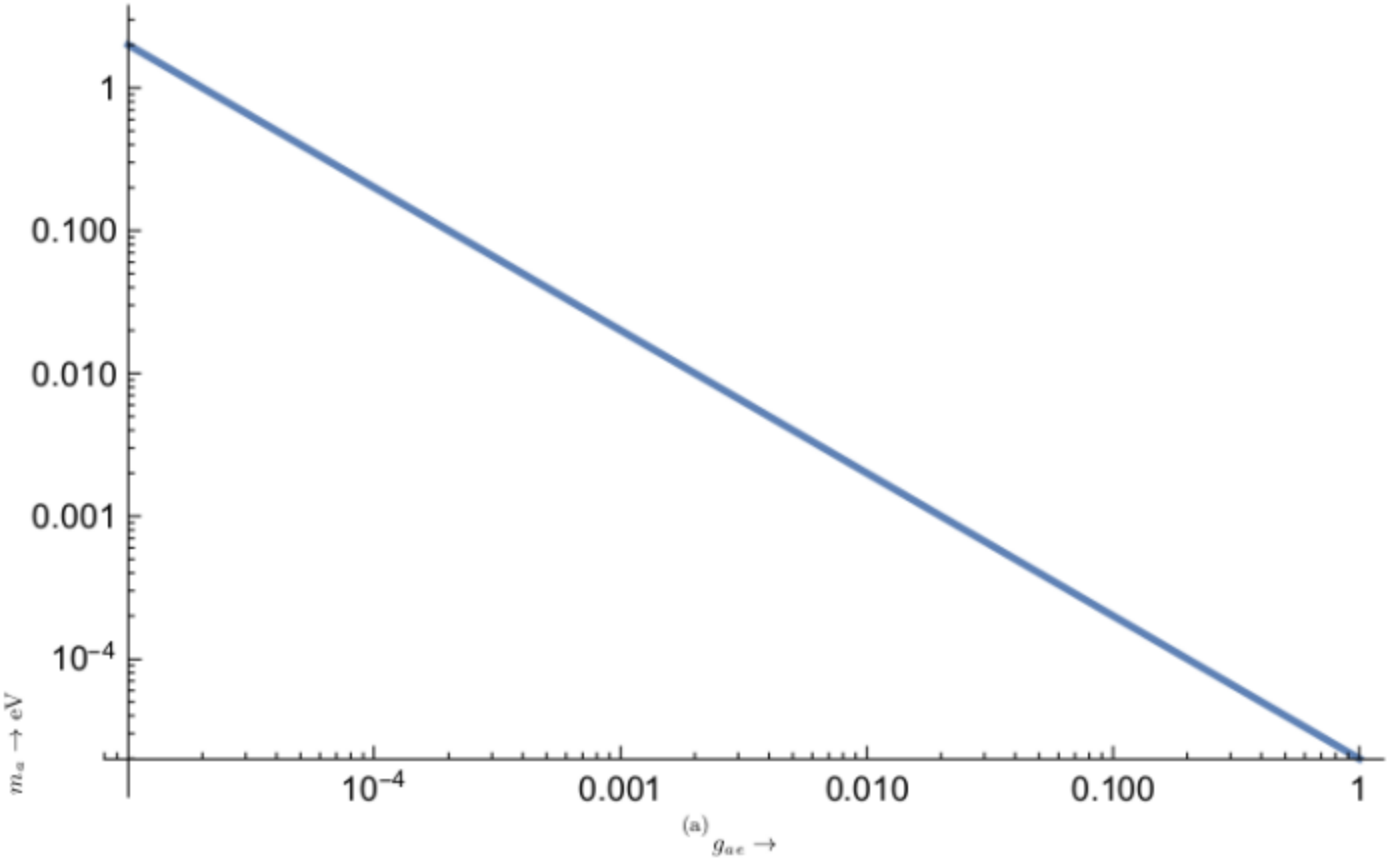

# -The cross section is given by:

$$\sigma = \frac{1}{v}\frac{1}{2m_a}\left(\frac{g_e}{2f_a}\right)^2 (C_{\ell,j_1,m_1,j_2,m_2})^2 \left(\delta_{m_1,m_2}q_0^2 + \frac{1}{2}(q_1^2+q_2^2)(1-\delta_{m_1,m_2})\right) 2\pi\delta(m_a + \frac{q^2}{2m_a} + E_i - E_f) \quad (8)$$

We will now fold the cross section with the axion velocity distribution, assuming that with respect to the galactic center is of the Maxwell-Boltzmann type:

$$f_g(v') = \frac{1}{v_0^3}\frac{1}{\pi\sqrt{\pi}} e^{-\left(\frac{v'}{v_0}\right)^2} \quad (9)$$

In the local frame, ignoring for the moment the motion of the Earth, we have $\boldsymbol{v}' \to \boldsymbol{v} + v_0\hat{z}$

$$f_\ell(\boldsymbol{v}) = \frac{1}{v_0^3}\frac{1}{\pi\sqrt{\pi}} e^{-\left(y^2+2y\xi+1\right)},\ y = \frac{v}{v_0} \quad (10)$$

# - Folding the cross section with the velocity distribution (continued)

The integration over the velocity distribution we find:

$$\langle y\sigma \rangle = \frac{1}{2m_a}\left(\frac{g_e}{2f_a}\right)^2 (C_{\ell,j_1,m_1,j_2,m_2})\,\Lambda$$

$$\Lambda = 4\sqrt{\pi} m_a \frac{1}{v_0} F_{m_1,m_2}(y),\ F_{m_1,m_2}(y) =$$
$$\frac{1}{2} y e^{-y^2-1} \begin{cases} \frac{1}{2}\left(\left(2y^2+1\right)\sinh(2y) - 2y\cosh(2y)\right), & m_1 = m_2 \\ \frac{1}{4}(2y\cosh(2y) - \sinh(2y)), & m_1 \neq m_2 \end{cases} \quad (15)$$

# -An expression for the rate

The rate for for N atoms in the target becomes

$$R = R_0(m_a)\,(C_{\ell,j_1,m_1,j_2,m_2})^2\,F_{m_1,m_2}(y),$$

$$R_0(m_a) = \Phi_0(m_a)\sigma_0, \Phi_0(m_a) = N\frac{\rho_a}{m_a}\upsilon_0, \sigma_0 = 2\sqrt{\pi}\frac{1}{\upsilon_0}\frac{g_{ae}^2}{f_a^2} \quad (18)$$

where $\Phi_a$ is the axion flux given by $\Phi_a = \frac{\rho_a}{m_a}\upsilon_0$ with $\rho_a = 0.3\text{Gev/cm}^3$ the axion density in our vaccinity. This leads to a large axion particle density $\frac{\rho_a}{m_a}$ due to the smallness of the axion mass.
This way $R_0(m_a)$ is written as a product of two constants, one with the dimension of the flux, which varies inversely proportional to the axion mass and the other yields the scale of the cross section.

The spin matrix element can be cast in form:

$$C_{L,J_1,m_1,J_2,m_2} = \langle {}^3L_{J_2m_2}|\sigma|{}^3L_{J_1m_1}\rangle$$
$$= \frac{1}{\sqrt{2J_2+1}}\langle J_1m_1, 1m_2 - m_1|J_2m_2\rangle\langle {}^3L_{J_2}||\sigma||{}^3L_{J_1}\rangle \quad (32)$$

# -Resonance behavior

In order to see the resonance behavior is better to present the functions $F$ as a function of the axion mass. To this end we note that $F = F_{m_1,m_2}(y)$ and $m_a = \Delta/(1 + (1/2)v_0^2 y^2)$. Thus the needed equation is given parametrically with the help of these two functions. It is just more convenient to use $\frac{\Delta}{m_a} - 1$, $\Delta = E_2 - E_1$, instead of $m_a$, see Fig, 6.

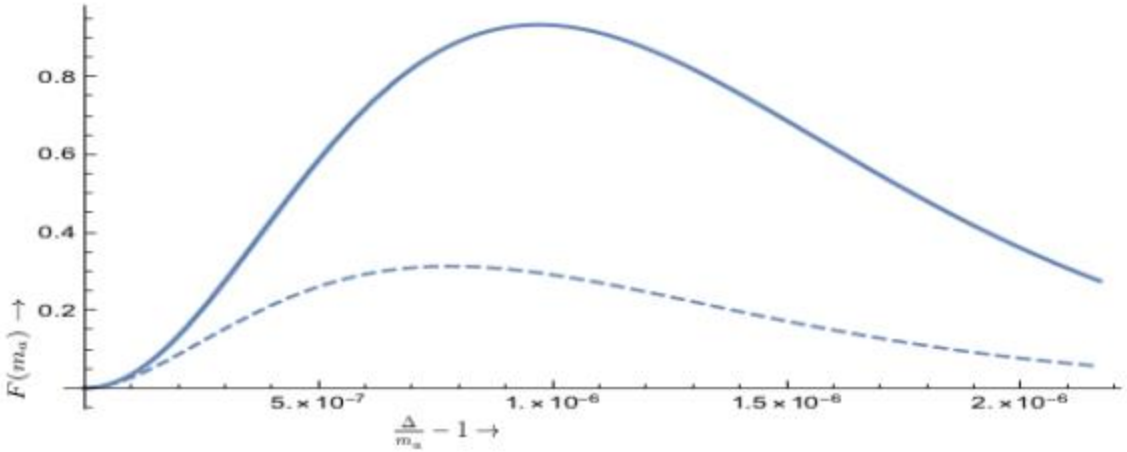


FIG. 6: The cross section exhibits resonance behavior. Shown is $F(X) \rightarrow F(m_a)$ as a function of $\frac{\Delta}{ma} - 1$ The solid line corresponds to $m_1 = m_2$, while the dashed line corresponds to $m_1 \neq m_2$, both in the local frame.

# -The scale of the rate $R_0(m_a)$

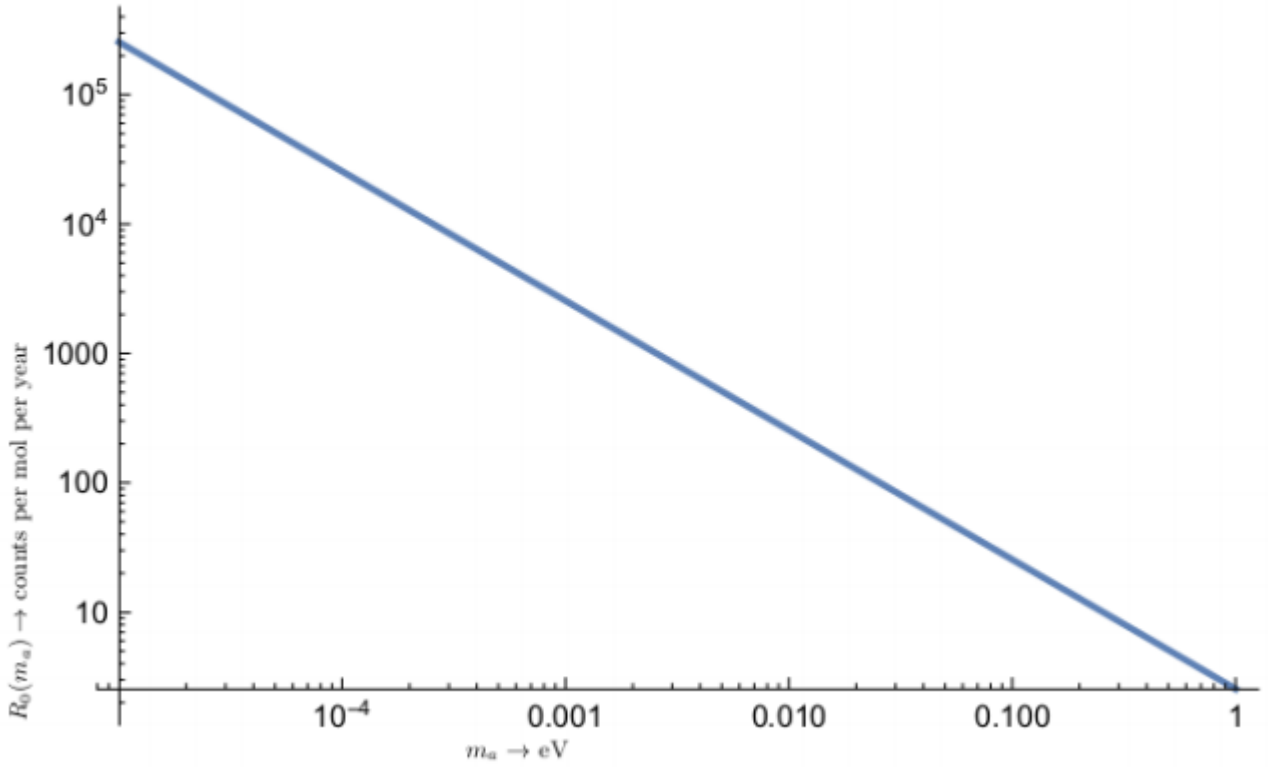


FIG. 3: The scale of the rate as a function of the axion mass.

# - Rates obtained for some special targets of interest

In all cases the most important parameters are:

I) The splitting due to the magnetic moment given in terms of

$$\delta = 57.85\ (B/1T)\mu eV$$

ii) The spin orbit splitting ε determined experimentally. Typically in the range of a few meV

- s (angular momentum zero) states. The splitting is 2δ: δ=57.85 (B/1T)μeV. The width: Γ=0.7x10$^{-6}$

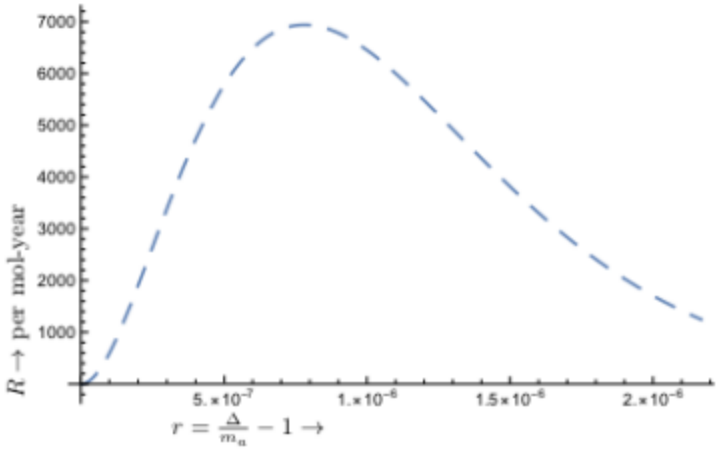


FIG. 8: The only possible transition is of $A$ type. Now the transition energy is $\Delta = 6 \times 10^{-5} \frac{B}{1\mathrm{T}}(1+r)$ eV. The extracted axion mass is given by the value of $r_0$ at the location of the maximum, $m_a = m_A(1-r_0)$, $m_A = 2\delta$. The width is determined by $\Gamma = r_2 - r_1$, where $r_2$ and $r_1$ the locations at half maximum.

Target $_{13}Al$ (single particle p states);

$\delta$=57.85 (B/1T)μeV



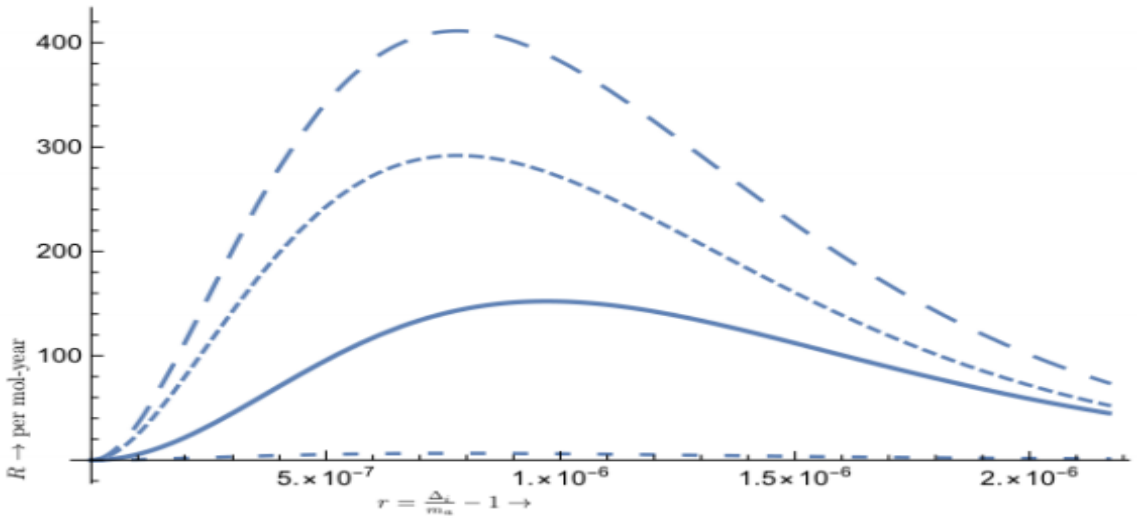


FIG. 9: The rate as a function of $r = \frac{\Delta}{m_a} - 1$, for transition types $A$, $B$, $C$, $D$ indicated by long dash, short dash, solid line and intermediate dash respectively. Note that to make the type $A$ fit in the picture we have suppressed it by the factor $C_g = 1/5$, i.e. its actual value ia 5 times larger. The extraction of the axion mass and the resonance widths are determined as follows: $r_0 \to r_0^i$, $r_1 \to r_1^i$ and $r_2 \to r_2^i$, $m_a(i) \leftrightarrow m_i(1 - r_0^i)$, $i = A, B.C, D$. The parameters $m_i$ are $m_A = \frac{2\delta}{3}$, $m_B = \epsilon - \frac{5\delta}{3}$, $m_C = \epsilon - \frac{\delta}{3}$, $m_D = \delta + \epsilon$. In the case of $_{13}$Al considered here $\epsilon = 0.0130$ eV. For any other single particle p-orbitals only $\epsilon$ may be different.

Target $_{21}Sc$ (single paricle d states). $m_a(i)=(1-r^{ri}{}_0)m_i$, i=A, B, C, D

$\delta=57.85(B/1T)\mu eV$

From top to bottom A, B, C, D terms.

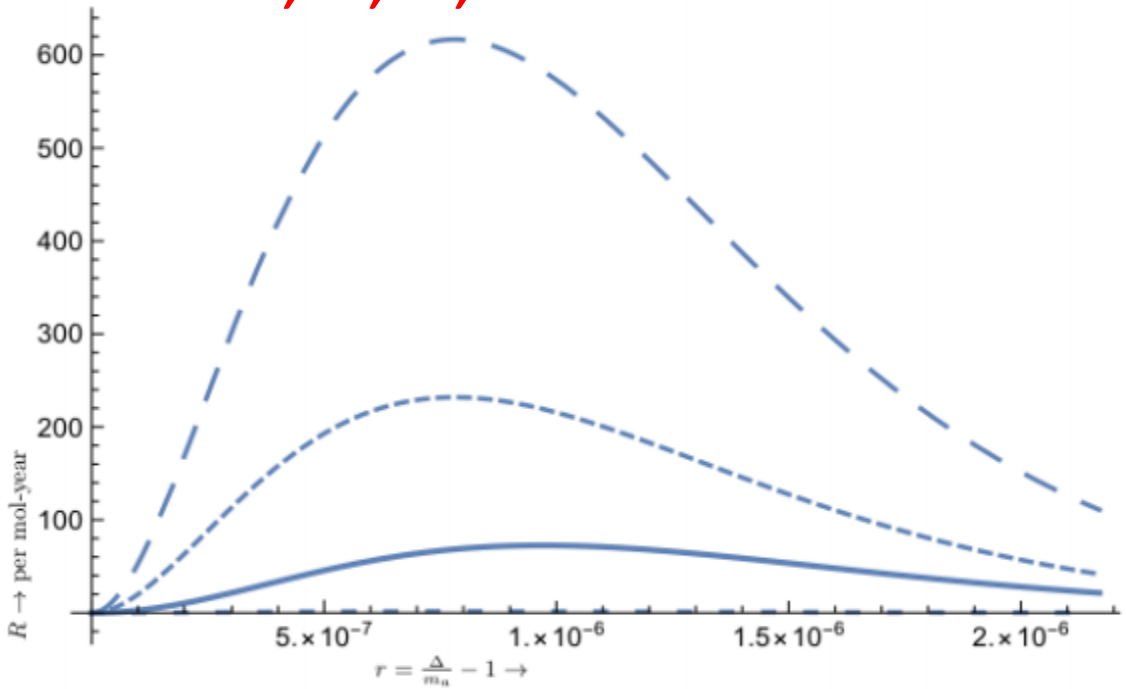


FIG. 10: The same as in Fig. 9 in the case of the atom $_{21}$Sc. The parameters $m_i$ are as follows: $m_A=\frac{8\delta}{5}$, $m_B=\epsilon-\frac{9\delta}{5}$, $m_C=\epsilon-\frac{3\delta}{5}$, $m_D=\epsilon+\frac{3\delta}{5}$, with $\epsilon=0.021$eV.

# Target Ti : 2 electron configuration; δ=57.85 (B/1T)μeV

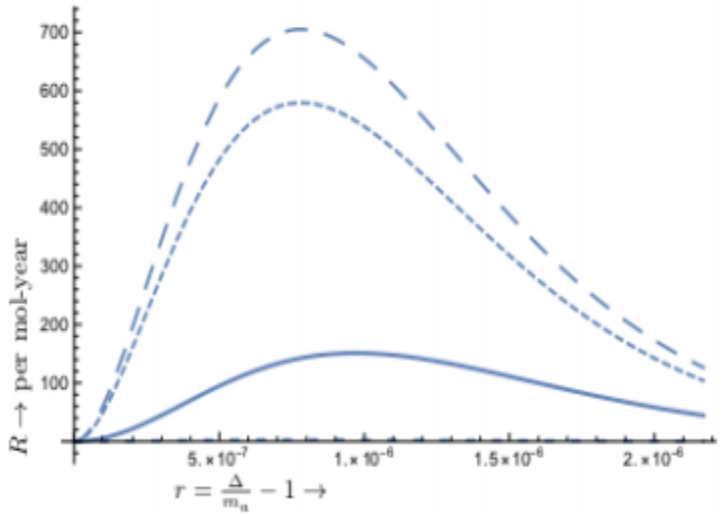


FIG. 14: The same as in Fig. 9 but for the Ti atom (the gs is of the form $4s^2 3d^2\, {}^3F_2$, while excited state that can be reached is ${}^3F_3$). For transition type $A$ the suppression factor $C_g = 1/5$ was employed, i.e the corresponding rate must be multiplied by 5. Now $m_i$ given by $m_A = \frac{28\delta}{9}$, $m_B = \frac{121\delta}{72} + \epsilon$, $m_C = \frac{115\delta}{36} + \epsilon$ , $m_D = \frac{113\delta}{24} + \epsilon$, $\epsilon = 0.02$ eV. The The type $D$ transition is not visible.

Target $_{26}$Fe. The transition is $^5D_4$ -> $^5D_3$ (3 electron system)
δ=57.85 (B/1T) μeV

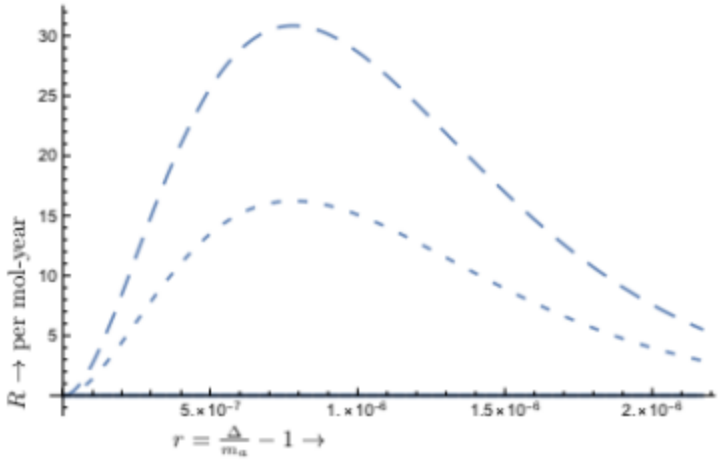


FIG. 16: The same as in Fig. 9 but for the iron target. The $A$ term has been suppressed by a factor of 1/500, i.e. its actual value is 500 larger. Now $m_i$, $i = A, D$ with $m_A = \frac{16}{5}\delta$, $M_D = \epsilon + \frac{16}{5}\delta$, $\epsilon = 0.05$ eV. The other two transition types $B$, $C$ do not occur.

# Temperature requirements for low axion mass

- **W**e have seen that that the final state of the transition must be empty.

It may, however, be accidentally populated due to Boltzmann factor:

$$P_{i,f} = e^{-m_a/kT} \tag{37}$$

Suppose that we demand this to be $10^{-x}$. Then we find that

$$T \leq \frac{0.434 m_a}{kx} \Rightarrow T \leq \frac{5000}{x}\frac{m_a}{1\text{eV}} \tag{38}$$

For light axions the experiment must done at very low temperature.

- One must make sure that the atomic properties of the target are retained at these temperatures.

This can be achieved for special materials or if the relevant atoms occur as impurities in the target.

- Temperature requirements versus the axion mass



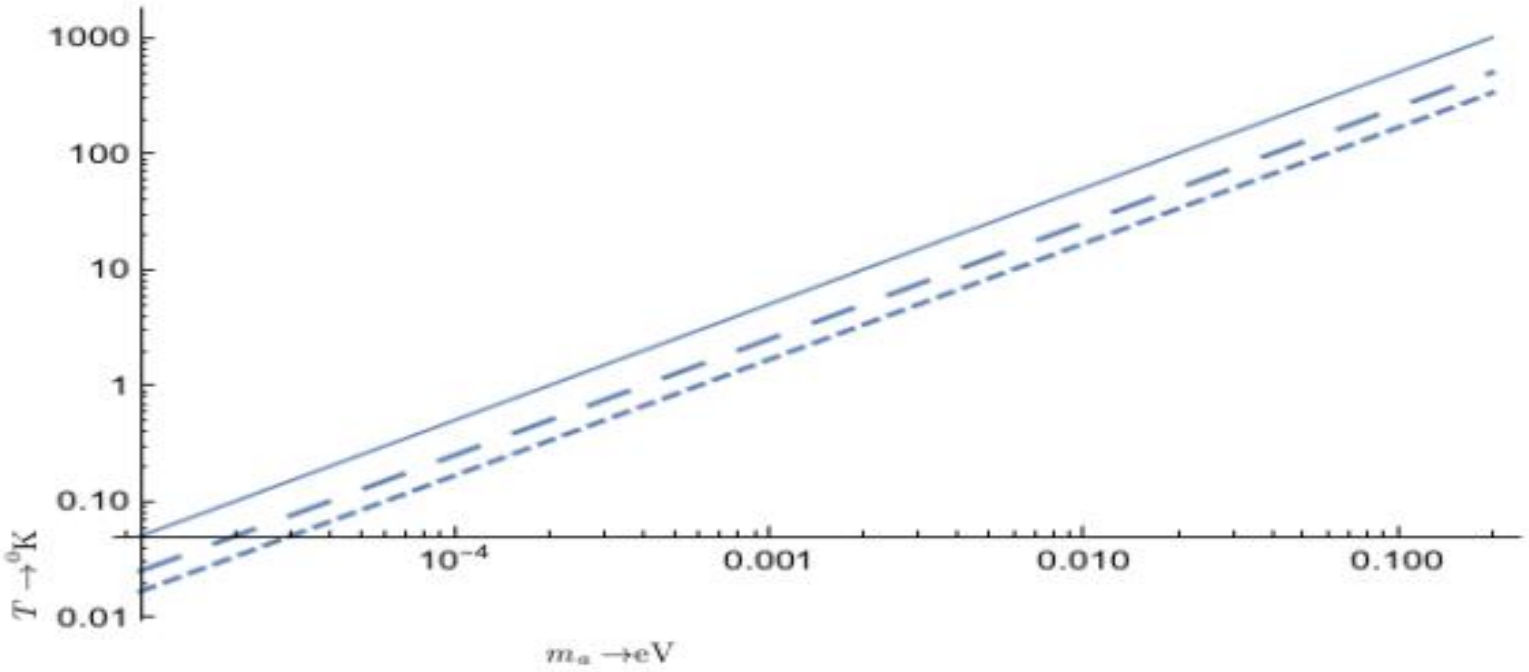


FIG. 7: The temperature in degrees Kelvin to be achieved is the region below the above curves, so that the population of the excited state by thermal electrons can be neglected. The continuous curve corresponds to relative probability of 10%, the long dash to 1% and the sort dash to 0.1%

# Dealing with the narrow width

- We have seen that in all atoms considered the expected resonances are very narrow. Since we have no experimental or theoretical information about the axion mass, the axion might be missed by experiments. The solution is to use an oscillating magnetic field

The oscillation period must be as short as possible and, in any case, very much shorter than the run time of the experiment.
The latter must be longer than the time implied by the predicted event rate to compensate for the fact that only a fraction of the time the equipment is going to be at the right state of sensitivity for axion detection. With this arrangement one can see the axion provided its mass lies between $m_i|\ B=B_{Bmin}$ and $m_i|\ B=B_{max}$ for i = A, B, C, D.

This range depends on the atom considered. The most favored case is the one with as large as possible magnetic moment splitting.
Thus, in the case of the iron target, one can detect light axion masses through the A term, with a rate 15000 $(\text{y-mol})^{-1}$ compared to 15 $(\text{y-mol})^{-1}$ of the D-term.

# Dealing with the narrow width (Sikivie's idea)

**This can lead to the range for the A-term:**

**$16/5\ (\delta/n) \leq m_a \leq (16/5)\ \delta$ =>2 μeV ≤ $m_a$ ≤ 0.2 meV,B=1 T, n=100**

**and: 0.05eV+2 μeV ≤ $m_a$ ≤ 0.05 eV+0.2 meV for D term**

**Sikivie's idea: Let say that |0> is the ground state and |1> is the state excited by the axion. The axion is inferred by the de- excitation |1> or, better still, by exciting |1> to a convenient level |2> via a tunable LASER. Then observe the de- excitation of |2> to a convenient level.**

**Thus the narrow windows of axion mass can be open in atomic physics detection, provided that the sweep in frequency is smooth and gap-less, exploiting the feasibility of simultaneous scan of the frequency of the LASER and the magnetic field in a prescribed way.**

**This way one would think that the narrowness of the signal is beneficial rather than problematic, yielding an advantage for the atomic experiments.**

# Concluding Remarks

1. Axion to photon conversion:ADMX, CAPP (Center for Axion and Precision Physics Research)

Some exclusion plots (ADMX experiment):

**$2.66\ \mu eV \leq m_a \leq 2.81\ \mu eV$ (PRL 120, 151301 (2018))**

**$2.81\ \mu eV \leq m_a \leq 3.31\ \mu eV$ (PRL 124, 101303 (2020))**

2. Axion absorption in atomic excitations (this proposal).

By a suitable choice of the target large detectable rates are expected.

By a suitable choice of the atom and the magnetic field a variety of axion masses may be detected

In the same run:

a) Axion masses in the range tens of μeV can be detected via the A term and b) masses in the range of tens of meV can be detected via the B, C, D terms.

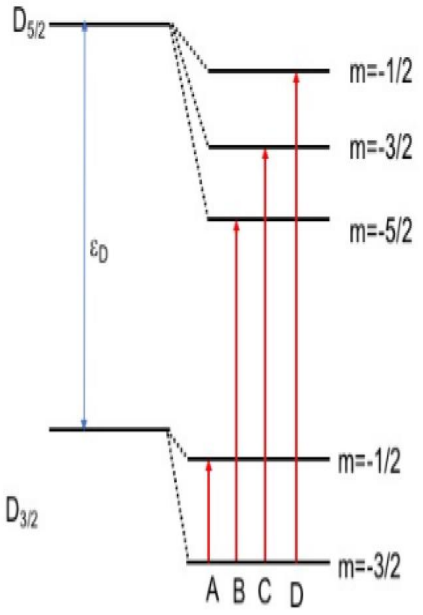

# THE END

# Why axions? They are good dark matter candidates!

The relic axions produced during the QCD phase transition in the early Universe satisfy all the requirements of dark matter. Thus the hypothetical axion solves simultaneously both the strong CP and dark matter problems.

In the scenario in which the PQ symmetry breaks before cosmological inflation (pre- inflation scenario), the relic axion abundance is determined only by the initial amplitude ($\theta_0$) and the mass of the axion field. The abundance of dark matter in the Lambda cold dark matter model is naturally explained by an axion mass above ~0.1 μeV for ($\theta_0$)> 0.1.

In the post-inflation scenario, where the PQ symmetry breaks after cosmological inflation, most calculations suggest that the axion mass lies in the range 1–100 μeV, see e.g., S. Borsanyi, et al, Nature (London) 539, 69 (2016).

# Dealing with the narrow width (Sikivie's idea)

**This can lead to the range for the A-term:**

**$16/5\ (\delta/n) \leq m_a \leq (16/5)\ \delta$ =>2 μeV ≤ $m_a$ ≤ 0.2 meV,B=1 T, n=100**

**and: 0.05eV+2 μeV ≤ $m_a$ ≤ 0.05 eV+0.2 meV for D term**

**The width of the resonance becomes larger if a larger magnetic field is used.**

**Sikivie's idea: Let say that |0> is the ground state and |1> is the state excited by the axion. The axion is inferred by the de- excitation |1> or, better still, by exciting |1> to a convenient level |2> via a tunable LASER. Then observe the de- excitation of |2> to a convenient level.**

**Thus the narrow windows of axion mass can be open in atomic physics detection, provided that the sweep in frequency is smooth and gap-less, exploiting the feasibility of simultaneous scan of the frequency of the LASER and the magnetic field in a prescribed way.**

**This way one would think that the narrowness of the signal is beneficial rather than problematic, yielding an advantage of the atomic experiments**

# Temperature requirements for low axion mass

- **W**e have seen that that the final state of the transition must be empty.

It may, however, be accidentally populated due to Boltzmann factor:

$$P_{i,f} = e^{-m_a/kT} \tag{37}$$

Suppose that we demand this to be $10^{-x}$. Then we find that

$$T \leq \frac{0.434 m_a}{kx} \Rightarrow T \leq \frac{5000}{x}\frac{m_a}{1\text{eV}} \tag{38}$$

For light axions the experiment must done at very low temperature.

- One must make sure that the atomic properties of the target are retained at these temperatures.

This can be achieved for special materials or if the relevant atoms occur as impurities in the target.

# Neutron Electric Dipole Moment

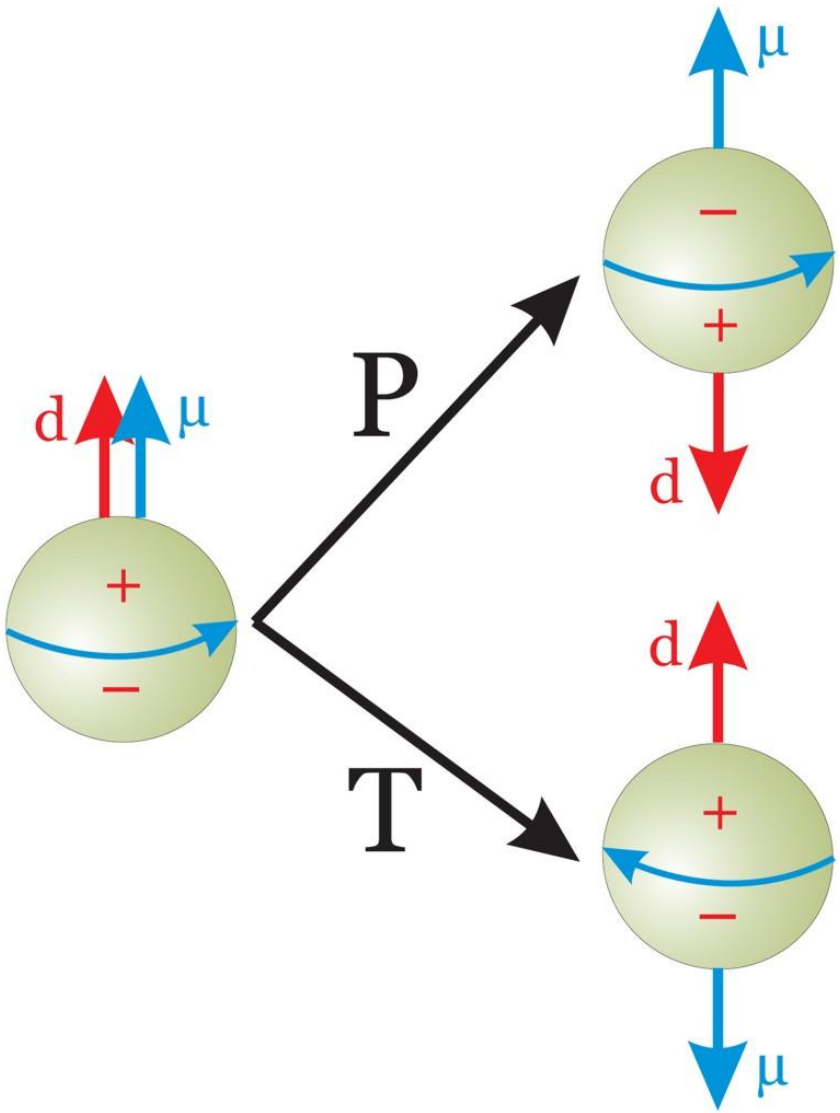


Violates time reversal (T) and space reflection (P) symmetries

Natural scale

$$\frac{e}{2m_N} = 1.06 \times 10^{-14} ecm$$

Experimental limit

$$|d| = 0.63 \times 10^{-25} ecm$$

Limit on coefficient

$$\overline{\Theta}\frac{m_q}{m_N} \lesssim 10^{-11}$$

# Two realistic axion models

- **THE KIM-SHIFMAN-VAINSHTEIN-ZAKHAROV (KSVZ) AXION**. The SM is expanded to include a singlet scalar and heavy quark doublet. As above one gets couplings to the gluons and the EM field.
- **THE DINE-FISCHLER-ZITNITSKY (DFZ) AXION.** It extends the S-M with two Higgs doublets. Lagrangian has a global P-Q chiral symmetry $U_{PQ}(1)$, which is spontaneously broken, generating a Goldstone boson, the axion (a).

# Top: Photon to axion conversion
# bottom: Axion induced atomic excitation

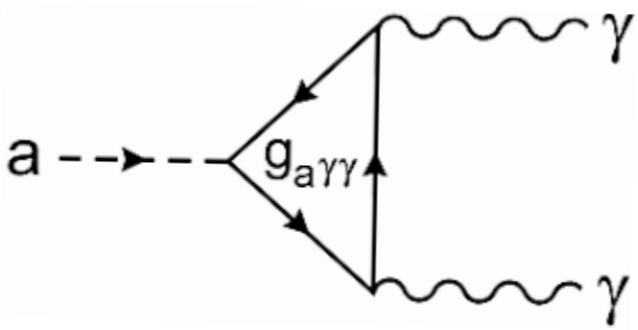


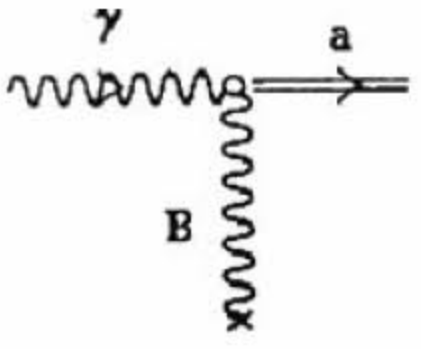


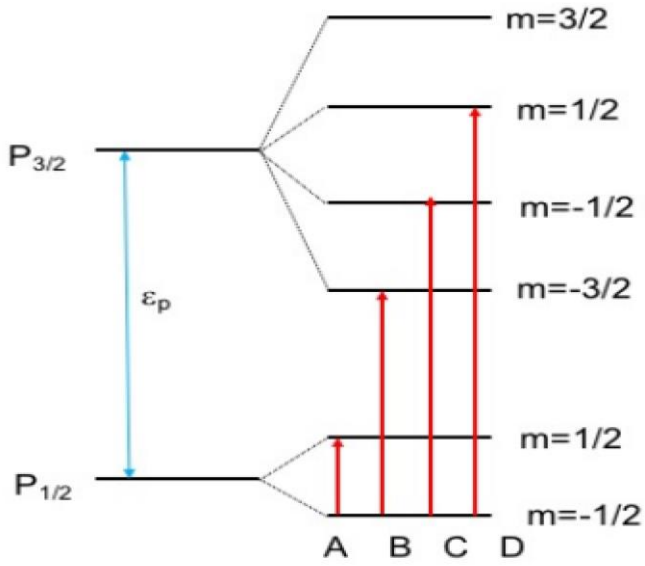


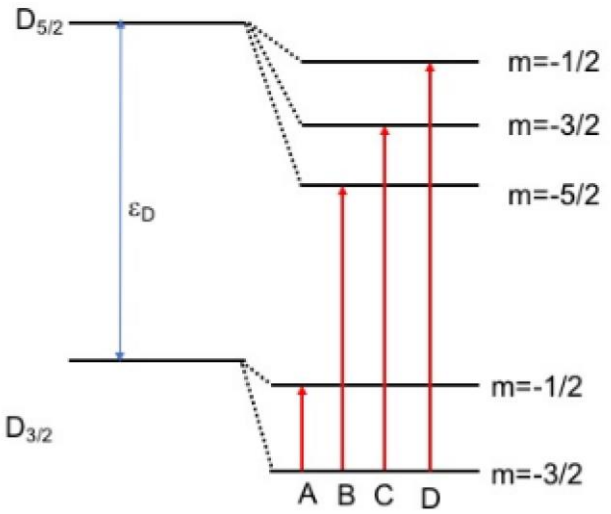

top:Photon to axion conversion

bottom: Axion induced atomic excitation

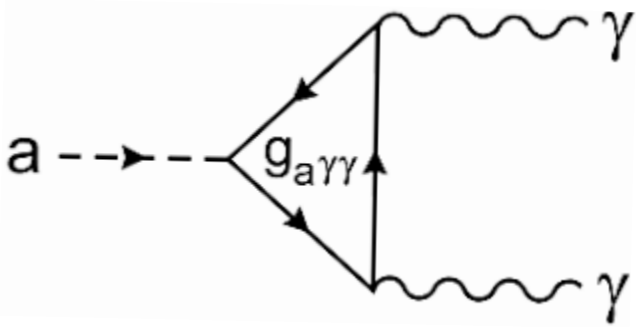


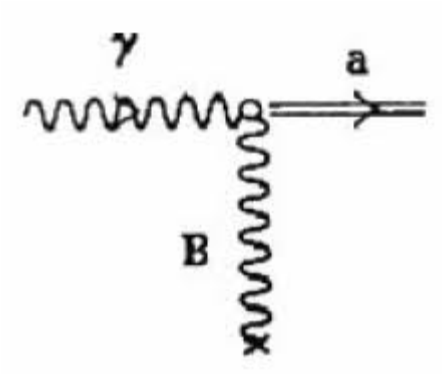


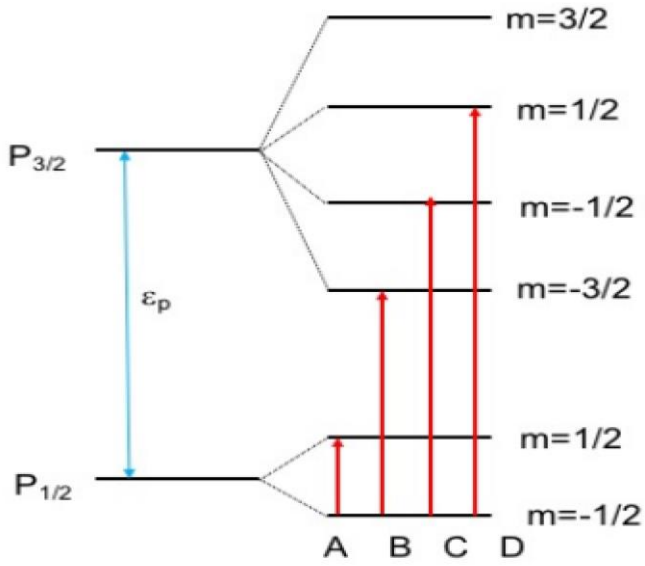


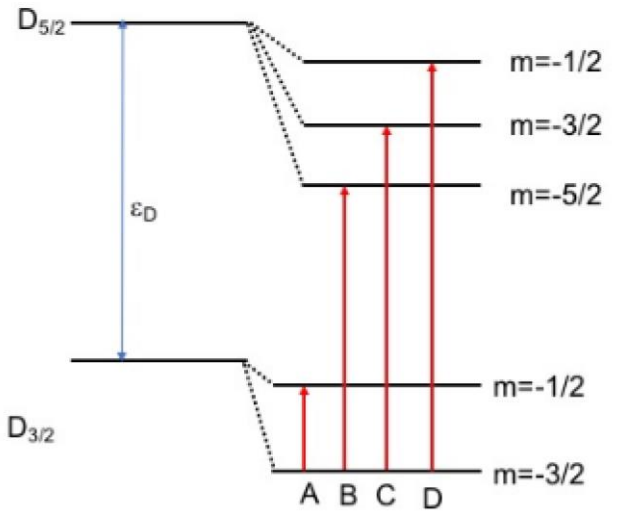

top:Photon to axion conversion

bottom: Axion induced atomic excitation

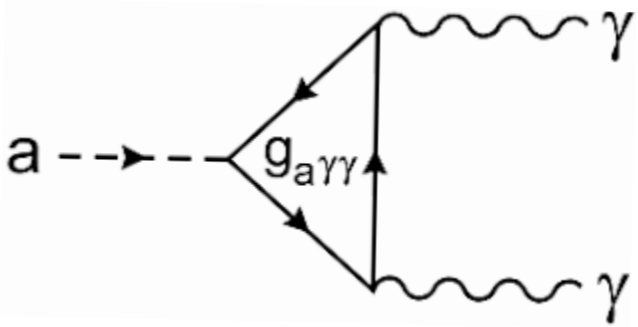


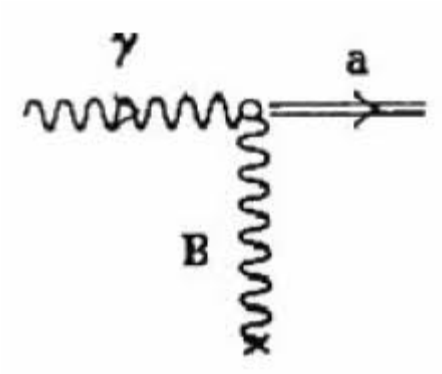


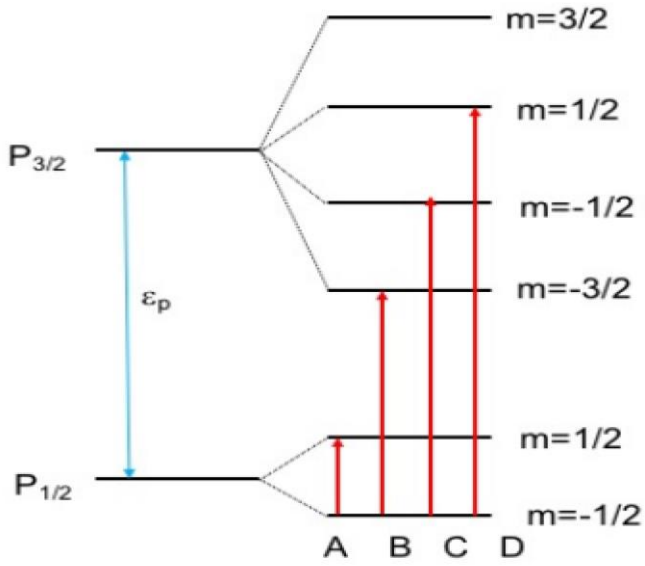


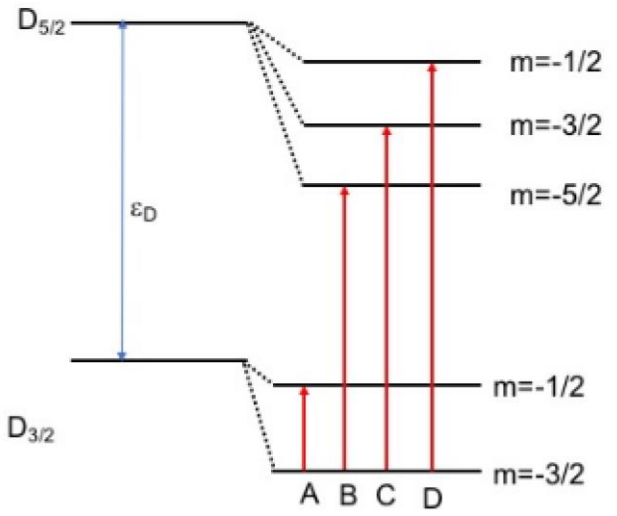

# axion searches

- The axion field is **homogeneous** over a large de Broglie wavelength.
- oscillating in a coherent way <-> ideal cold dark matter candidate in the mass range

  $10^{-6}$ eV<$m_a$ <$10^{-3}$ eV
- Their mass is small, but they are non relativistic. Their number density in the galaxy is very large
- They are being searched by resonant cavities (ADMX etc, CAPP)
- Heavier axions with larger mass 1eV produced thermally ( $a\pi\pi\pi$ etc ), e.g. in the sun, are also interesting and are searched by CERN Axion Solar Telescope (CAST)
- Detection of axions in the μeV as well eV range may also be detected using atomic physics processes at low temperatures.
- In the eV range the temperatures need not be very low, so ordinary atoms may be used.
- In μeV range the temperatures have to be near the absolute zero. So some exotic materials need be employed. Such as
- super atoms
- Artificial atoms
- Manganese-Doped ZnSe Nanocrystals
- NV (nitrogen vacancies) in diamond
- So in this case one can search for axions other than dark matter as well.
- Other axion like particles (ALPs), with broken symmetries not connected to QCD, and dark photons form dark matter candidates called WISPs (Weakly Interacting Slim Particles) can be searched by atomic physics experiments

# The axion as dark matter candidate

The relic axions produced during the QCD phase transition in the early Universe satisfy all the requirements of dark matter. Thus the hypothetical axion solves both the strong CP and dark matter problems.

In the scenario in which the PQ symmetry breaks before cosmological inflation (pre- inflation scenario), the relic axion abundance is determined only by the initial amplitude ($\theta_0$) and the mass of the axion field. The abundance of dark matter in the Lambda cold dark matter model is naturally explained by an axion mass above ~0.1 μeV for ($\theta_0$)> 0.1.

In the post-inflation scenario, where the PQ symmetry breaks after cosmological inflation, most calculations suggest that the axion mass lies in the range 1–100 μeV, see e.g., S. Borsanyi, et al, Nature (London) 539, 69 (2016).

# Axion Like Particle Searches -
## ADMX &CAPP (Dark Mtter) and CAST (solar axions)

**Detection with resonant cavities (axion - photon coupling). ADMX: red. QCD axions <-> hatched band**

**Regions of interest in the $(m_a, g_{a\gamma\gamma})$ plane**

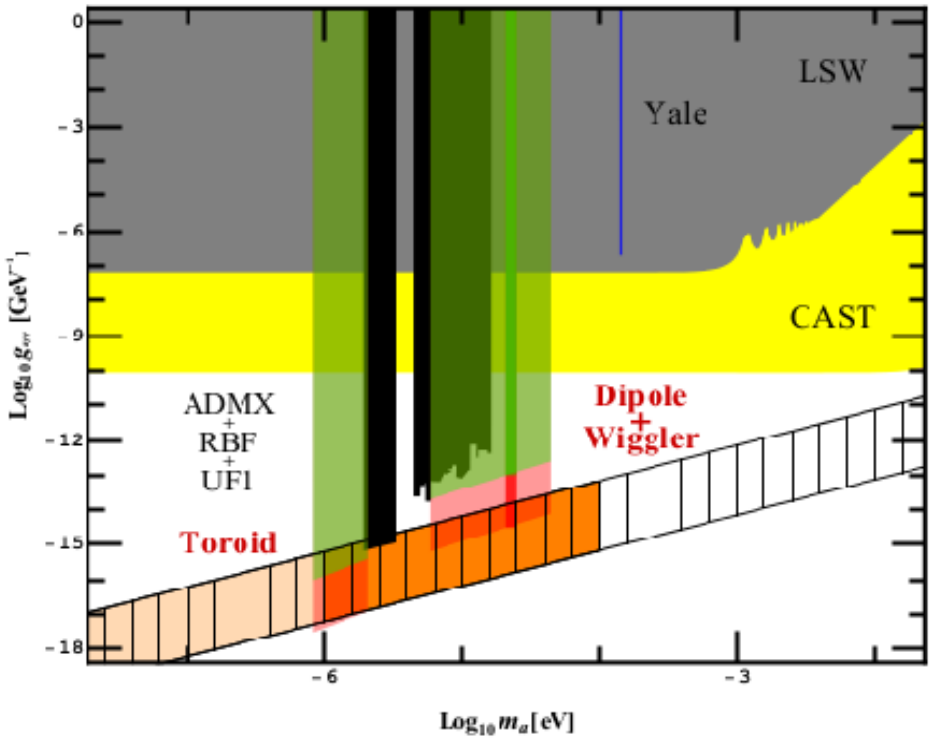


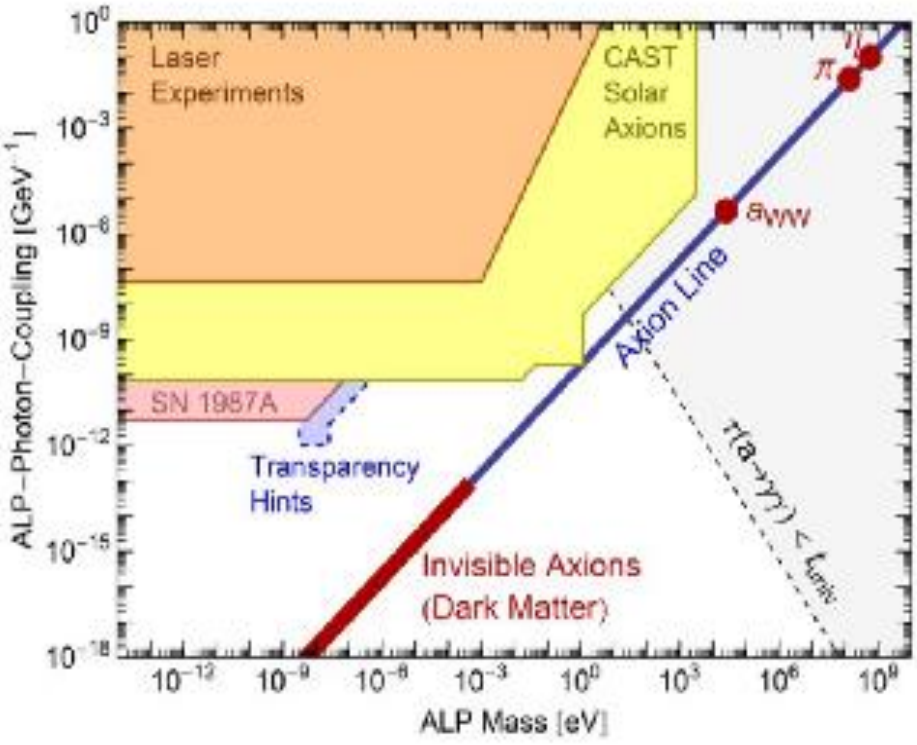

- Consider an atom with three levels:
- Level 1 fully occupied by electrons
- Level 2 completely empty of electrons (at low temperature)
- Level 3 a convenient level to be reached by photon excitation from a tunable laser
- An axion comes in and promotes an electron from level 1 to level 2
- The tunable laser promotes this electron to level 3
- The de-excitation of level 3 manifests the presence of the axion

# The relevant matrix element

## between m-sub-states (split in a magnetic

$$\langle n\ell j_2 m_2|\mathbf{q}.\boldsymbol{\sigma}|n\ell j_1 m_1 = \langle j_1\, m_1, 1\, m_2 - m_1|j_2\, m_2\rangle\sqrt{(2j_1+1)3}\sqrt{2\ell+1}\sqrt{6}\begin{Bmatrix} \ell & \frac{1}{2} & j_1 \\ \ell & \frac{1}{2} & j_2 \\ 0 & 1 & 1 \end{Bmatrix}(-1)^{m_1-m_2} q_{m_1-m_2} I_{n\ell}(\mathbf{q}) \quad (1)$$

expressed in terms of the Glebsch-Gordan coefficient and the nine- j symbol.

$$I_{n\ell}(\mathbf{q}) = \int d^3\mathbf{p}\phi_{n\ell}(\mathbf{p}+\mathbf{q})\phi_{n\ell}(\mathbf{p})$$

Since the momentum transfer $\mathbf{q}$ is small $I_{n\ell}(\mathbf{q}) \approx 1$. So the matrix element becomes

$$|ME(\mathbf{q})|^2 = \left(\frac{g_e}{2f_a}\right)^2 (C_{\ell,j_1,m_1,j_2,m_2})^2 \left(\delta_{m_1,m_2} q_0^2 + \frac{1}{2}(q_1^2+q_2^2)(1-\delta_{m_1,m_2})\right) \quad (2)$$

where

$$C_{\ell,j_1,m_1,j_2,m_2} = \langle j_1\, m_1, 1\, m_2 - m_1|j_2\, m_2\rangle\sqrt{(2j_1+1)3(2\ell+1)6}\begin{Bmatrix} \ell & \frac{1}{2} & j_1 \\ \ell & \frac{1}{2} & j_2 \\ 0 & 1 & 1 \end{Bmatrix}(-1)^{m_1-m_2}$$

# Evaluation of the cross section

The cross section becomes

$$\sigma = \frac{1}{v}\frac{1}{2m_a}|ME(\mathbf{q})|^2 \int\int \frac{d^3\mathbf{p}'}{(2\pi)^3}(2\pi)^3\delta(\mathbf{p}+\mathbf{q}-\mathbf{p}')2\pi\delta(m_a+\frac{q^2}{2m_a}+E_i-E_f)$$

or

$$\sigma = \frac{1}{v}\frac{1}{2m_a}\left(\frac{g_e}{2f_a}\right)^2 (C_{\ell,j_1,m_1,j_2,m_2})^2 \left(\delta_{m_1,m_2}q_0^2+\frac{1}{2}(q_1^2+q_2^2)(1-\delta_{m_1,m_2})\right) 2\pi\delta(m_a+\frac{q^2}{2m_a}+E_i-E_f)$$

Then the event rate is given by:

$$R = \Phi_a\sigma = \frac{\rho_a}{m_a}v\sigma = \frac{\rho_a}{m_a}\frac{1}{2m_a}\left(\frac{g_e}{2f_a}\right)^2 (C_{\ell,j_1,m_1,j_2,m_2})^2 \left(\delta_{m_1,m_2}q_0^2+\frac{1}{2}(q_1^2+q_2^2)(1-\delta_{m_1,m_2})\right)$$
$$2\pi\delta(m_a(1+\frac{1}{2}v^2)+E_i-E_f) \qquad (3)$$

# The atomic physics factors

$$\left(\begin{array}{ccccc|c} \ell & j_1 & m_1 & j_2 & m_2 & C^2_{j_1,m_1,j_2,m_2,\ell} \\ \hline 0 & \frac{1}{2} & -\frac{1}{2} & \frac{1}{2} & \frac{1}{2} & 2 \end{array}\right),$$

$$\left(\begin{array}{cccc|cc|c} & |i\rangle & & |f\rangle & & & \\ \ell & j_1 & m_1 & j_2 & m_2 & C^2_{j_1,m_1,j_2,m_2,\ell} \\ \hline 1 & \frac{1}{2} & -\frac{1}{2} & \frac{1}{2} & \frac{1}{2} & \frac{2}{3} \\ 1 & \frac{1}{2} & -\frac{1}{2} & \frac{3}{2} & -\frac{3}{2} & \frac{1}{3} \\ 1 & \frac{1}{2} & -\frac{1}{2} & \frac{3}{2} & -\frac{1}{2} & \frac{2}{3} \\ 1 & \frac{1}{2} & -\frac{1}{2} & \frac{3}{2} & \frac{1}{2} & 0 \\ 1 & \frac{1}{2} & \frac{1}{2} & \frac{3}{2} & -\frac{1}{2} & \frac{1}{3} \\ 1 & \frac{1}{2} & \frac{1}{2} & \frac{3}{2} & \frac{1}{2} & \frac{2}{3} \\ 1 & \frac{1}{2} & \frac{1}{2} & \frac{3}{2} & \frac{3}{2} & 0 \\ 1 & \frac{3}{2} & -\frac{3}{2} & \frac{3}{2} & -\frac{1}{2} & \frac{1}{3} \\ 1 & \frac{3}{2} & -\frac{1}{2} & \frac{3}{2} & \frac{1}{2} & \frac{2}{3} \\ 1 & \frac{3}{2} & \frac{1}{2} & \frac{3}{2} & \frac{3}{2} & \frac{1}{3} \end{array}\right)$$

$$\left(\begin{array}{cccc|cc|c} & |i\rangle & & |f\rangle & & & \\ \ell & j_1 & m_1 & j_2 & m_2 & C^2_{j_1,m_1,j_2,m_2,\ell} \\ \hline 2 & \frac{3}{2} & -\frac{3}{2} & \frac{3}{2} & -\frac{1}{2} & \frac{6}{25} \\ 2 & \frac{3}{2} & -\frac{3}{2} & \frac{3}{2} & \frac{1}{2} & \frac{2}{25} \\ 2 & \frac{3}{2} & -\frac{3}{2} & \frac{3}{2} & \frac{3}{2} & \frac{16}{25} \\ 2 & \frac{3}{2} & -\frac{1}{2} & \frac{3}{2} & -\frac{3}{2} & \frac{4}{25} \\ 2 & \frac{3}{2} & -\frac{1}{2} & \frac{3}{2} & -\frac{1}{2} & \frac{8}{25} \\ 2 & \frac{3}{2} & -\frac{1}{2} & \frac{3}{2} & \frac{1}{2} & \frac{24}{25} \\ 2 & \frac{3}{2} & -\frac{1}{2} & \frac{3}{2} & \frac{3}{2} & \frac{3}{25} \\ 2 & \frac{3}{2} & \frac{1}{2} & \frac{3}{2} & -\frac{3}{2} & \frac{24}{25} \\ 2 & \frac{3}{2} & \frac{1}{2} & \frac{3}{2} & -\frac{1}{2} & \frac{12}{25} \\ 2 & \frac{3}{2} & \frac{1}{2} & \frac{3}{2} & \frac{1}{2} & \frac{6}{25} \\ 2 & \frac{3}{2} & \frac{1}{2} & \frac{3}{2} & \frac{3}{2} & \frac{12}{25} \\ 2 & \frac{3}{2} & \frac{3}{2} & \frac{3}{2} & -\frac{1}{2} & \frac{24}{25} \\ 2 & \frac{3}{2} & \frac{3}{2} & \frac{3}{2} & \frac{1}{2} & \frac{24}{25} \\ 2 & \frac{3}{2} & \frac{3}{2} & \frac{3}{2} & \frac{3}{2} & \frac{4}{25} \\ 2 & \frac{3}{2} & -\frac{3}{2} & \frac{5}{2} & \frac{3}{2} & \frac{16}{25} \\ 2 & \frac{3}{2} & -\frac{1}{2} & \frac{5}{2} & \frac{1}{2} & \frac{8}{25} \\ 2 & \frac{3}{2} & \frac{1}{2} & \frac{5}{2} & \frac{3}{2} & \frac{12}{25} \\ 2 & \frac{5}{2} & -\frac{5}{2} & \frac{5}{2} & -\frac{3}{2} & \frac{16}{25} \\ 2 & \frac{5}{2} & -\frac{3}{2} & \frac{5}{2} & -\frac{1}{2} & \frac{18}{25} \\ 2 & \frac{5}{2} & -\frac{1}{2} & \frac{5}{2} & \frac{1}{2} & \frac{16}{25} \\ 2 & \frac{5}{2} & \frac{1}{2} & \frac{5}{2} & \frac{3}{2} & \frac{2}{5} \end{array}\right)$$

## - Exotic materials super atoms, Artificial atoms, $NV^-$ (see [21]<->Phys. Rep. 528 (2013)1)

It amusing to note that one may be able to employ at low temperatures some exotic materials used in quantum technologies (for a recent review see [21]) like nitrogen-vacancy (NV), i.e. materials characterized by spin $S = 1$, which in a magnetic field allow transitions between $m = 0$, $m = 1$ and $m = -1$. These states is spin symmetric. Antisymmetry requires the space part to be antisymmetric, i.e. a wave function of the form

$$\psi = \phi^2_{n\ell}(r)\,[L = \text{odd}, S = 1]\; J = L - 1, L, L + 1$$

Of special interest are:

$$\psi = \phi^2_{n\ell}(r)\,{}^3P_J, \phi^2_{n\ell}(r)\,{}^3F_J$$

Then the spin matrix element takes the form:

$$\langle {}^3L_{J_2 m_2}|\sigma|{}^3L_{J_1 m_1}\rangle = \frac{1}{\sqrt{2J_2+1}}\langle J_1 m_1, 1 m_2 - m_1|J_2 m_2\rangle \langle {}^3L_{J_2}||\sigma||{}^3L_{J_1}\rangle,\; L = P, F$$

The reduced matrix elements are given in table III. the full matrix element $\langle {}^3P_{J_2 m_2}|\sigma|{}^3P_{J_1 m_1}\rangle^2$ for the most important case is also shown in III

TABLE III: The coefficients $\langle {}^3P_{J_2}||\sigma||{}^3P_{J_1}\rangle$, $\langle {}^3F_{J_2}||\sigma||{}^3F_{J_1}\rangle$ and $\langle {}^3P_{J_2 m_2}|\sigma|{}^3P_{J_1 m_1}\rangle^2$. For the notation see text.

| $J_1$ | $J_2$ | $\langle {}^3P_{J_2}\|\|\sigma\|\|{}^3P_{J_1}\rangle$ |
|---|---|---|
| 0 | 1 | $\sqrt{\frac{2}{3}}$ |
| 1 | 1 | $\frac{1}{\sqrt{2}}$ |
| 1 | 2 | $\sqrt{\frac{5}{6}}$ |
| 2 | 2 | $\sqrt{\frac{5}{2}}$ |

| $J_1$ | $J_2$ | $\langle {}^3F_{J_2}\|\|\sigma\|\|{}^3F_{J_1}\rangle$ |
|---|---|---|
| 2 | 2 | $-\frac{\sqrt{10}}{3}$ |
| 2 | 3 | $\frac{2\sqrt{5}}{3}$ |
| 3 | 3 | $\frac{\sqrt{7}}{6}$ |
| 3 | 4 | $\frac{3}{2}$ |
| 4 | 4 | $\frac{\sqrt{15}}{2}$ |

| $J_1$ | $m_1$ | $J_2$ | $m_2$ | $\langle {}^3P_{J_2 m_2}\|\sigma\|{}^3P_{J_1 m_1}\rangle^2$ |
|---|---|---|---|---|
| 0 | 0 | 1 | $m_2$ | $\frac{2}{9}$ |
| 1 | $-1$ | 1 | $-1$ | $\frac{1}{6}$ |
| 1 | $-1$ | 1 | 0 | $\frac{1}{6}$ |
| 1 | 0 | 1 | 0 | 0 |
| 1 | 0 | 1 | 1 | $\frac{1}{6}$ |
| 1 | 1 | 1 | 1 | $\frac{1}{6}$ |

# Dealing with the narrow width (Sikivie's idea)

**This can lead to the range for the A-term:**

**$16/5\ (\delta/n) \leq m_a \leq (16/5)\ \delta$ =>2 μeV ≤ $m_a$ ≤ 0.2 meV,B=1 T, n=100**

**and: 0.05eV+2 μeV ≤ $m_a$ ≤ 0.05 eV+0.2 meV for D term**

**The width of the resonance becomes larger if a larger magnetic field is used.**

**Sikivie's idea: Let say that |0> is the ground state and |1> is the state excited by the axion. The axion is inferred by the de- excitation |1> or, better still, by exciting |1> to a convenient level |2> via a tunable LASER. Then observe the de- excitation of |2> to a convenient level.**

**Thus the narrow windows of axion mass can be open in atomic physics detection, provided that the sweep in frequency is smooth and gap-less, exploiting the feasibility of simultaneous scan of the frequency of the LASER and the magnetic field in a prescribed way.**

**This way one would think that the narrowness of the signal is beneficial rather than problematic, yielding an advantage of the atomic experiments**